

Chapter 6.

OPTIMIZED CROSS SECTION DESIGNS

The research work described in this chapter is partly based on the following papers :

1. R.C. Gupta, S.A. Kahn and G.H. Morgan, *Coil and Iron Design for SSC 50 mm Magnet*, Proceedings of the 1990 American Society of Mechanical Engineers (ASME) Winter Annual Meeting in Dallas (1990).
2. R.C. Gupta, S.A. Kahn and G.H. Morgan, *A Comparison of Calculations and Measurements of the Field Harmonics as a Function of Current in the SSC Dipole Magnets*, Proceedings of the 1991 IEEE Particle Accelerator Conference, San Francisco, pp. 42-44 (1991).
3. R.C. Gupta, et al., *RHIC Insertion Magnets*, Proceedings of the 1991 IEEE Particle Accelerator Conference, San Francisco, pp. 2239-2241 (1991).
4. R.C. Gupta, S.A. Kahn and G.H. Morgan, *SSC 50 mm Dipole Cross section*, Proceedings of the International Industrial Symposium on Super Collider (IISCC), Atlanta, pp. 587-600 (1991).
5. R. Gupta, et al., *Large Aperture Quadrupoles for RHIC Interaction Regions*, Proceedings of the 1993 Particle Accelerator Conference, Washington, D.C., pp. 2745-2747 (1993).
6. R.C. Gupta, A.K. Jain, *Variation in a_1 saturation in SSC Collider Dipoles*, Proceedings of the 1993 Particle Accelerator Conference, Washington, D.C., pp. 2778-2780 (1993).
7. R. Gupta, et al., *Field Quality Improvements in Superconducting Magnets for RHIC*, Proceedings of the 1994 European Particle Accelerator Conference, London, UK, pp. 2928-2930 (1994).

6.1. Introduction

In this chapter the magnetic design and optimization process and the final design of the cross section of the 130 mm aperture RHIC insertion quadrupole and the prototype of the 50 mm aperture SSC dipole magnet will be described. The field harmonics of the SSC dipole magnet are specified for a reference radius of 10 mm and is given in units of 10^{-4} of the central field. The harmonics of the insertion quadrupole are specified for a reference radius of 40 mm, in units of 10^{-4} of the field magnitude at this radius.

6.2. SSC 50 mm Aperture Collider Dipole Magnet Cross-section

In this section the magnetic design of the two dimensional coil and iron cross section for the prototype 50 mm aperture main ring dipole magnet for the Superconducting Super Collider (SSC) is presented. Several prototype dipole magnets based on this design have been built at Brookhaven National Laboratory (BNL) and at Fermi National Accelerator Laboratory (FNAL). Except for a few minor differences (which will be discussed in more detail later), the magnetic design of the BNL and FNAL magnets is nearly the same. The computed values of the allowed field harmonics as a function of current, the quench performance predictions, the stored energy calculations, the effect of construction errors on the field harmonics and the Lorentz forces on the coil will be discussed. The yoke has been optimized to reduce the effects of iron saturation on the field harmonics. A summary of this design will also be presented.

6.2.1. Coil Design

The coil is made of two layers of superconducting cables. Some parameters of the cables used in the inner and outer layers are given in Table 6.2.1.

The coil is designed by placing the cables in such a way that they produce a field with a high degree of uniformity. This is done using the computer program PAR2DOPT [130] which uses analytic expressions for computing the field harmonics at the center of the magnet of coils in a circular $\infty\mu$ iron aperture. It also computes the peak field on the surface of the conductor.

A large number of configurations for the coil design were examined. The one selected has a total of 45 turns in each quadrant in two layers. The inner layer has 19 turns in four blocks (three wedges) and the outer has 26 turns in two blocks (one wedge). In the final selection of the optimized coil cross section, the peak field (the maximum magnitude of the magnetic field in the conductor) was also used as an important parameter in addition to the other magnetic and mechanical parameters. For the same transfer function, a coil design with a lower peak field will produce a magnet which will quench at a higher current. In a search for the optimum coil configuration, the number of wedges in the outer layer was kept at one whereas for the inner layer, solutions with a variable number of wedges were examined. The designs with two wedges in the inner layer were, in general, found to have a higher peak field or excessive harmonic content. For this reason, the design chosen

Table 6.2.1: Properties of the cables used in the SSC 50 mm dipoles. J_c gives the value of the critical current density which was used in the design calculations for the superconducting part of the wires (strands) and cables.

Cable parameters	Inner layer	Outer Layer
Filament diameter, micron	6.0	6.0
Strand diameter, mm	0.808	0.648
Strand $J_c(5T, 4.2K)$, A/mm^2	2750	2750
No. of strands	30	36
No. of strands \times Strand Area, mm^2 (area of metal)	15.382	11.872
Cable $J_c(5T, 4.2K)$, A/mm^2	2612.5	2612.5
Cable width, bare, mm	12.34	11.68
Cable width, insulated, mm	12.51	11.85
Cable mid-thickness, bare, mm	1.458	1.156
Cable mid-thickness, insulated, mm	1.626	1.331
Cable area, bare, mm^2	17.99	13.50
Cable area, insulated, mm^2	20.34	15.77
Keystone, (max-min) thickness, mm	0.262	0.206

has three wedges in the inner layer. However, the present coil is optimized in such a way that the two wedges nearest to the pole in the inner layer are identical and symmetric. A symmetric wedge design has a lower chance of incorrect installation as compared to a non-symmetric wedge design. The final design with symmetric wedges has performance comparable to those that did not require the wedges to be symmetric. The wedge in the outer layer is close to symmetric and in fact, in magnets built at FNAL this wedge was also made mechanically symmetric, without changing its effective size in the coil.

The cross section of the optimized coil placed in the stainless steel collar is shown in Fig. 6.2.1.

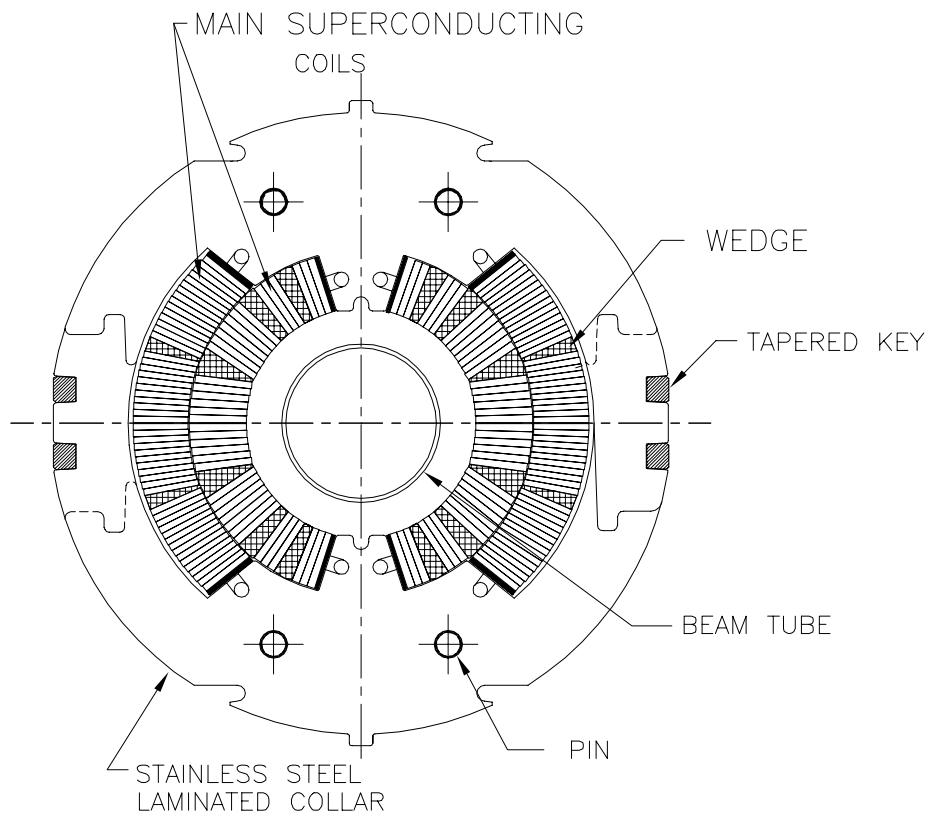


Figure 6.2.1: The cross section of the optimized coil for the prototype SSC 50 mm main collider dipole magnet. The coil is shown inside the stainless steel collar, which provides the compression on the coil.

6.2.2. Low Field Harmonics

The iron aperture is not completely circular in this magnet. It has a pole notch and a small vertical straight face at the midplane. These features introduce small but noticeable values of the b_2 and b_4 harmonics. These harmonics should be cancelled in the coil design if the magnet is to produce zero low field harmonics. Therefore, to cancel the effects of the non-circular iron inner radius, -0.28 unit of b_2 and $+0.01$ of b_4 were desired in the optimized coil. In addition, a non-zero value of b_8 harmonic was desired for centering the coil during the field measurements. Since the given tolerance in b_8 was 0.05 unit at the time of design, a solution was sought which had a magnitude for this harmonic between 0.04 and 0.05 . This requirement on b_8 eliminated many coil configurations from contention. However, the final design that satisfied all of the above requirements was equal in performance to those that did not. An alternate cross section with a zero b_8 harmonic was also designed which was mechanically very close to this cross section and, moreover, had all wedges perfectly symmetric. However, no magnet was ever built with this alternate cross section.

In Table 6.2.2 the desired and optimized values of field harmonics are presented. Harmonics higher than b_{12} had an optimized value of < 0.001 , as desired. In the row labelled "Desired" the allowed systematic errors are also listed. In the row "BNL magnets", the harmonics include the effects of the pole notch and the flat face in the iron at the midplane. These would be the expected values of low field harmonics in this magnet, not including the contributions from persistent currents in the superconductor. The size of the cable used in the actual magnets was different (inner layer cable wider and outer layer cable thinner) by a small amount from that assumed in the original design. This produced noteworthy deviations in the three lowest allowed field harmonics. The last two rows of the table, "Revised BNL" and "Revised FNAL", refer to the values of field harmonics in the magnet after this change in the cable size.

A small difference in the "Revised BNL" and "Revised FNAL" harmonics is due to the fact that (a) the pole angle in the outer layer of the FNAL cross section is 10 mil (0.254 mm) smaller than in the BNL version (the wedge size was the same therefore the effective cable thickness in the coil was reduced) and (b) the notch in the aperture of the vertically split iron is at the midplane and in the horizontally split iron is at the pole. The normalization or reference radius (R_0) for the field harmonics is 10 mm and as usual the harmonics are given in units 10^{-4} of the central field.

Table 6.2.2: Desired and Optimized values of *low field* harmonics with a circular aperture. The harmonics in “BNL magnets” include the effects of the pole notch and a flat face in the iron at the mid-plane. These harmonics are in units of 10^{-4} at 10 mm reference radius. The last two rows include the effects of a change in cable size.

Values	b_2	b_4	b_6	b_8	b_{10}	b_{12}
Desired	$-.28 \pm .4$	$.01 \pm .1$	$0 \pm .05$	$\pm .045 \pm .05$	$0 \pm .05$	$0 \pm .05$
Optimized	-0.280	0.009	-0.004	0.044	0.014	-0.001
BNL magnets	0.000	-0.001	-0.004	0.044	0.014	-0.001
Revised BNL	1.566	0.070	-0.024	0.043	0.015	-0.001
Revised FNAL	0.165	0.073	-0.021	0.043	0.015	-0.001

6.2.3. Iron Yoke Design

In this section, the process used in designing the iron yoke is discussed. The iron contributes about 22% to the magnetic field at 6.7 tesla (somewhat higher at lower field). Since the magnetization of the iron is not a linear function of the current in the coil and varies throughout the cross section, the uniformity of the field becomes a function of the current in the coil. The yoke is optimized to produce a minimum change in the field harmonics due to iron saturation for the maximum achievable value of transfer function at 6.7 tesla. The results of field computations with the computer codes POISSON and MDP will be presented here. The computer model of the final design and the results of field calculations with POISSON will be discussed in more detail. An iron packing factor of 97.5% has been used in these calculations.

If no special technique for controlling iron saturation were used, the change in the b_2 harmonic due to iron saturation would be over 1 unit. The following three options were considered for reducing the b_2 saturation swing. They all try to control the iron saturation at the iron aperture so that it saturates evenly.

- Reduced (shaved) iron o.d.
- Stainless Steel (non-magnetic) key at the midplane
- Shim at the iron inner surface

The first scheme, though most straight forward, produces a larger loss in transfer function at 6.7 tesla than the other two schemes. The third scheme, though actually increasing the transfer function at 6.7 tesla due to extra iron, requires more engineering development due to its non-circular aperture. The second scheme produces very little loss in transfer function (0.3% at 6.7 tesla compared to a keyless or magnetic key version) for a comparatively large reduction in b_2 due to saturation ($\frac{3}{4}$ unit). Moreover, it has the advantage of giving a way to control the b_2 due to saturation by changing the location and/or size of the key without affecting the other parts of the magnet design. It may be pointed out that besides the change due to iron saturation, b_2 and the other harmonics are also a function of current because of the coil deformation due to Lorentz forces. This has been observed in several SSC 40 mm aperture dipole magnets [64]. If the measured change in the b_2 harmonic is more than desired (either due to saturation or due to coil motion due to Lorentz forces), then this could be a useful and convenient method of correction.

The cross section of the cold mass (coil, collar and yoke) for the BNL-built SSC 50 mm prototype dipole is shown in Fig. 6.2.2. The POISSON model of this optimized cross section is given in a previous chapter as Fig. 3.2.2. The cross section for the vertically split iron used by FNAL is shown in Fig. 6.2.3. The field lines at 6500 ampere are also shown in this figure. The iron i.d. is 135.6 mm; leaving a space of 17 mm for the collar, and the iron o.d. is 330.2 mm. The stainless steel key in the horizontally split yoke design is located at 91.4 mm and has a size of 12.7 mm \times 12.7 mm. In the vertically split design for the FNAL-built magnet, a cutout at the horizontal midplane is incorporated to reduce iron saturation. The size and location of this cutout is the same as in the BNL yoke. As mentioned earlier, the iron aperture is not completely circular. The BNL yoke has a pole notch of size 5.11 mm \times 2.67 mm and a vertical straight face at the midplane which starts at $x = 67.13$ mm. The FNAL yoke has both the notch at the midplane and a vertical face at the midplane. The FNAL yoke has an additional pin located below the bus slot. This pin is made of non-magnetic steel and produces a noticeable effect on iron saturation. Other features in the two yokes are shown in the above mentioned figures.

The computed transfer function (T.F.) and b_2 as a function of current in the BNL and FNAL magnets are listed in Table 6.2.3. The b_2 harmonic has been adjusted so that it starts from zero; a non-zero value is artificial and is related to the way the computer model of a given coil and the iron geometry is set up in the two codes. The maximum computed b_2 due to saturation is about 0.3 unit. The calculations presented here, however, do not include

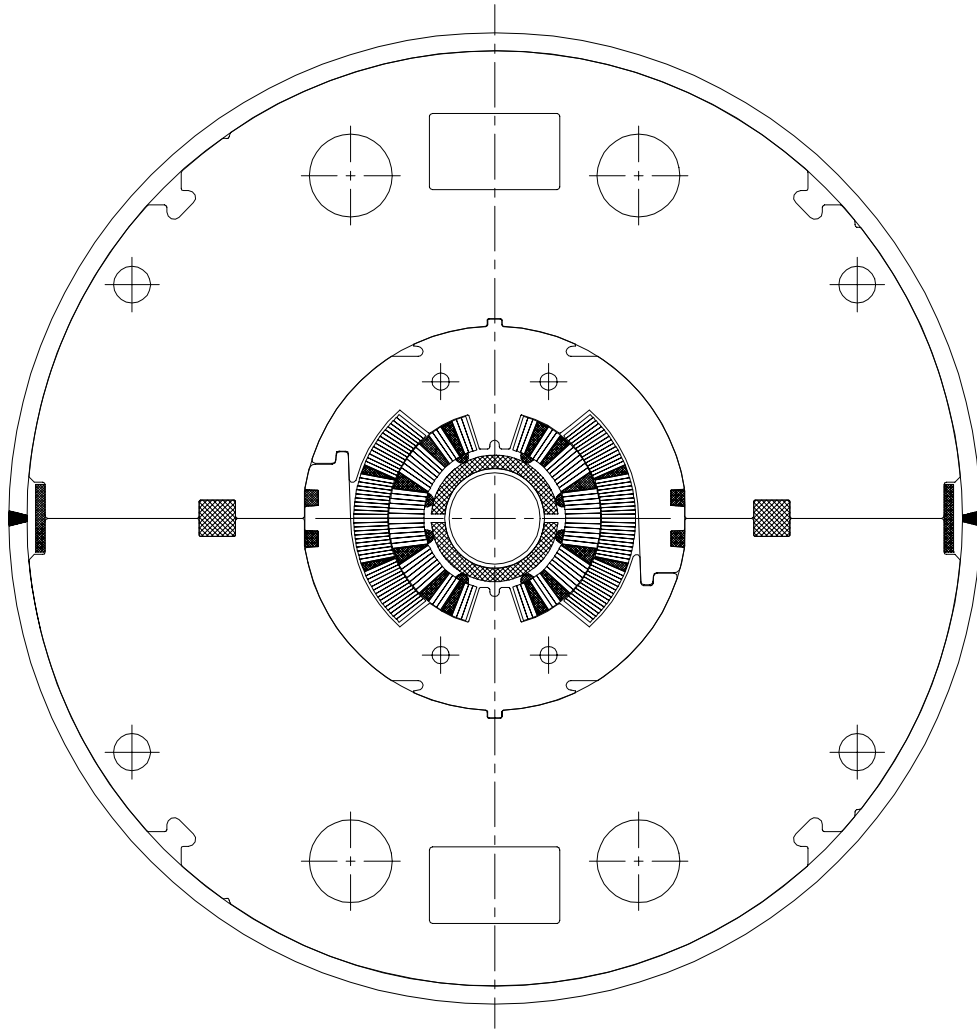


Figure 6.2.2: The cross section of the cold mass of 50 mm aperture horizontally split iron SSC arc dipoles. This cross section has been used in BNL built prototype magnets for SSC. The above cold mass is put inside a cryostat (not shown here).

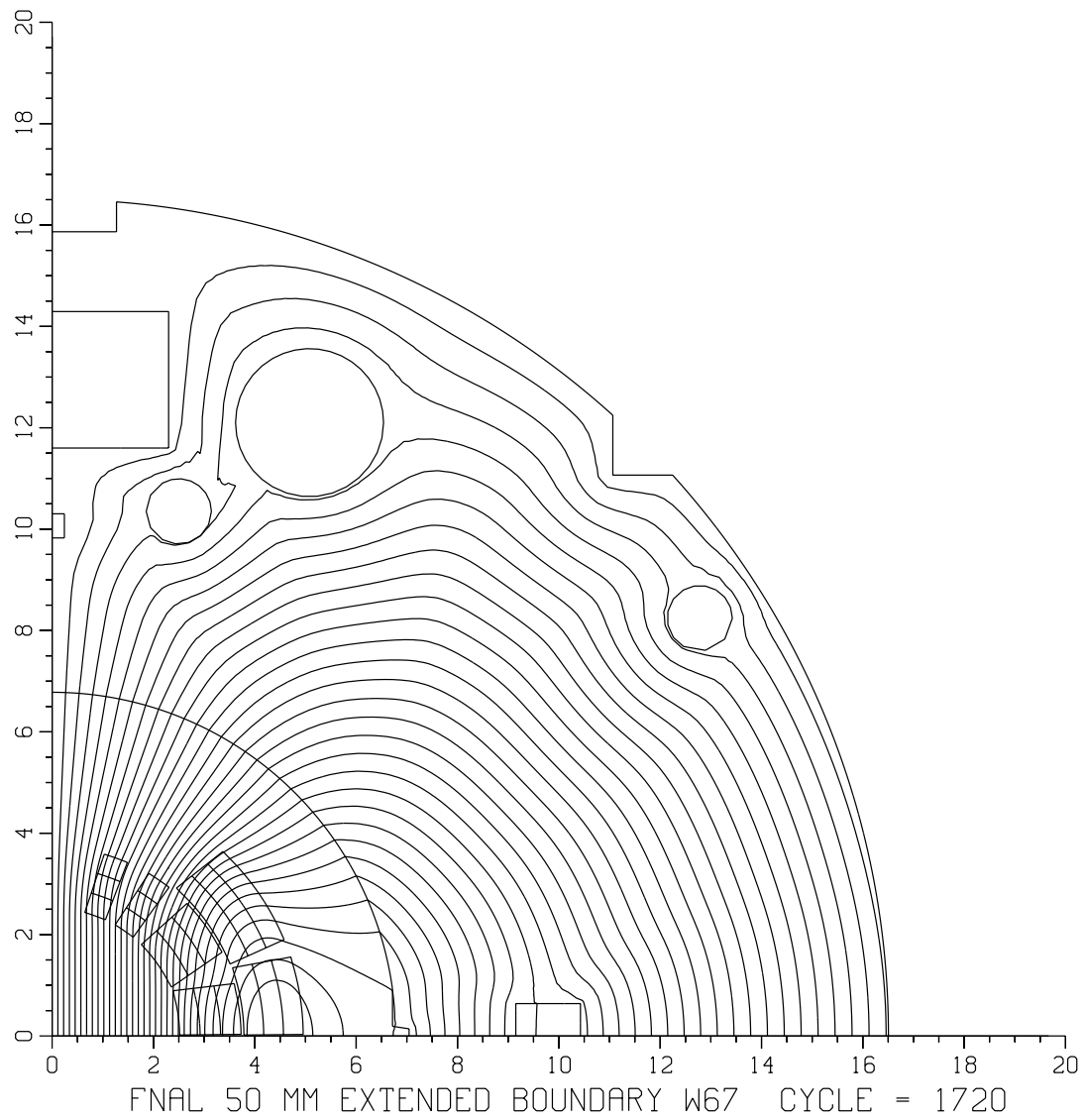


Figure 6.2.3: POISSON model and field lines at 6500 ampere for SSC 50 mm Dipole with vertically split iron laminations. This magnetic design was used in the prototype magnets built at FNAL.

the effects of the cryostat wall which modifies the current dependence of the harmonics at high current. POISSON uses a generalized finite difference method whereas MDP uses an integral method. Despite the fact that these two programs use two different methods for solving the problem, it is encouraging to see that both predict a small saturation shift. Similar calculations have been made by Kahn [64] with the computer code PE2D which uses the finite element method and good agreement has been found with the above calculations.

Table 6.2.3: Transfer function and b_2 variation as function of current. In all cases b_2 is corrected to start from zero at 3.0 kA. FNAL yoke calculations were done only with the code POISSON.

I kA	T.F. (T/kA)			$b_2 \times 10^{-4}$		
	FNAL yoke	BNL yoke		FNAL yoke	BNL yoke	
		POISSON	MDP		POISSON	MDP
3.0	1.0450	1.0447	1.0430	0.00	0.00	0.00
4.0	1.0445	1.0441	1.0413	-0.02	0.08	0.05
5.0	1.0398	1.0397	1.0364	-0.04	0.22	0.16
5.5	1.0339	1.0340	1.0311	0.19	0.26	0.21
6.0	1.0257	1.0262	1.0236	0.36	0.14	0.17
6.25	1.0209	1.0219	1.0194	0.38	0.07	0.11
6.5	1.0159	1.0173	1.0148	0.35	-0.03	0.03
7.0	1.0053	1.0073	1.0051	0.17	-0.33	-0.19
7.6	0.9926	0.9955	0.9935	-0.15	-0.77	-0.60
8.0	0.9845	0.9877	0.9861	-0.38	-1.06	-0.85
8.6	0.9732	0.9766	0.9758	-0.70	-1.43	-1.20

The maximum change in the b_2 and b_4 harmonics and the drop in transfer function, $\delta(TF)$, at 6.6 tesla (as compared to its value at low field) due to iron saturation as computed by these codes are listed in Table 6.2.4. All higher harmonics remain practically unchanged. In the case of the FNAL yoke, the computations have been done only with the code POISSON.

Table 6.2.4: Drop in transfer function at 6.6 tesla and the maximum change in b_2 and b_4 ; higher harmonics remain practically unchanged.

Harmonic	POISSON	POISSON	MDP
	FNAL yoke	BNL yoke	BNL yoke
$\delta(TF)$, at 6.6T	2.84%	2.62%	2.70%
$\delta(b_2)_{max}$, 10^{-4}	0.36	0.28	0.22
$\delta(b_4)_{max}$, 10^{-4}	0.02	-0.03	-0.02

In Table 6.2.5 the results of POISSON calculations are presented for various values of current in the BNL design. In Fig. 6.2.4, the variation in field harmonics as a function of central field is plotted.

The coldmass (see Fig. 6.2.2) is placed in the cryostat. To provide the maximum space for the support posts which minimizes the heat leak, the cold mass is placed above the center of the cryostat, which breaks the top-bottom symmetry. At high field, when the field lines can not be contained in the iron yoke, the cryostat provides an extra return path for flux. A top-bottom asymmetry in the magnet structure is then seen in the magnetic field. The most prominent harmonic to reflect this asymmetry is the skew quadrupole (a_1) term. The presence of the skew quadrupole harmonic at high field and methods to minimize it have been discussed in a previous chapter.

Table 6.2.5: Results of POISSON computations for the SSC 50 mm dipole with the horizontally split yoke design built at BNL.

I kA	B_o tesla	T.F. T/kA	b_2 10^{-4}	b_4 10^{-4}	b_6 10^{-4}	b_8 10^{-4}	b_{10} 10^{-4}	b_{12} 10^{-4}
$\infty\mu$	$\infty\mu$	1.04493	0.020	-0.046	0.000	0.047	0.015	-0.001
3.000	3.1341	1.04471	0.031	-0.046	0.001	0.047	0.015	-0.001
4.000	4.1762	1.04406	0.111	-0.050	0.001	0.047	0.015	-0.001
4.500	4.6921	1.04268	0.140	-0.055	0.001	0.047	0.015	-0.001
4.750	4.9464	1.04135	0.182	-0.060	0.001	0.047	0.015	-0.001
5.000	5.1985	1.03969	0.255	-0.063	0.001	0.047	0.015	-0.001
5.250	5.4454	1.03721	0.299	-0.066	0.001	0.047	0.015	-0.001
5.500	5.6871	1.03402	0.291	-0.069	0.001	0.048	0.015	-0.001
5.750	5.9240	1.03027	0.235	-0.071	0.001	0.048	0.015	-0.001
6.000	6.1573	1.02621	0.172	-0.073	0.000	0.048	0.015	-0.001
6.250	6.3868	1.02189	0.100	-0.073	0.000	0.048	0.015	-0.001
6.500	6.6121	1.01725	-0.003	-0.072	0.000	0.048	0.015	-0.001
7.000	7.0513	1.00733	-0.300	-0.072	0.000	0.049	0.015	-0.001
7.600	7.5654	0.99545	-0.738	-0.070	0.000	0.049	0.015	-0.001
8.000	7.9014	0.98767	-1.032	-0.068	0.000	0.050	0.015	-0.001
8.600	8.3984	0.97656	-1.403	-0.064	0.000	0.050	0.015	-0.001

Current dependence in BNL Built SSC 50 mm Prototype Dipole

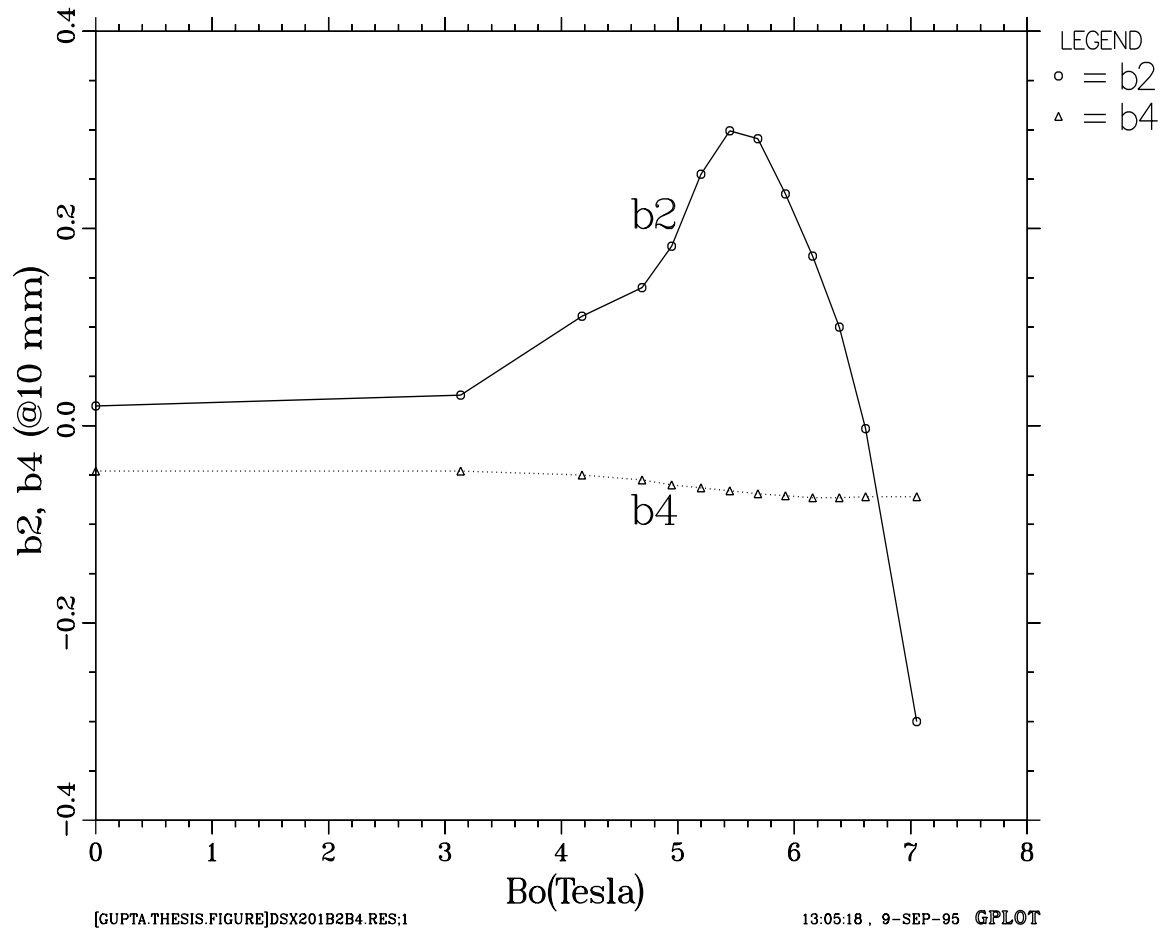


Figure 6.2.4: Variation in Field Harmonics as a function of Current in the SSC 50 mm BNL built prototype dipole magnet as computed by POISSON.

6.2.4. Expected Quench Performance

The central field at which a given cable loses its superconducting properties (B_{SS} , with “ss” standing for Short Sample) depends on the current in the cable which is a function of the maximum magnetic field at the conductor (the peak field) and the bath temperature. The superconducting cables for the inner and outer layers are optimized to provide a critical current (I_c) at a specified temperature and magnetic field. In a two layer coil design the magnetic design is optimized such that the computed short sample currents in the inner and outer layers are nearly the same. The peak field (B_{pk}) in the inner and outer layers of the SSC 50 mm dipole are listed in Table 6.2.6 for two values of central field (B_o). The ratio of B_{pk} to B_o , the *Enhancement Factor*, is given in the next column. In each layer, the peak field is found on the upper side of the top-most pole turn. The location of the peak field is listed in the next column. It is expressed as % of the cable width, measured from the upper-inner corner. The peak field calculations are done using the code MDP. MDP is based on the integral method and therefore is expected to give a more accurate field at the surface of the conductor as compared to codes based on the finite element method which require meshing the conductor.

Table 6.2.6: Peak fields in the SSC 50 mm dipole as computed using code MDP.

I	B_o	Inner			Outer		
		kA	tesla	B_{pk}, T	$\frac{B_{pk}}{B_o}$	Location	B_{pk}, T
6.85	6.9058	7.2374	1.048	5%	6.0016	0.869	11%
7.20	7.2100	7.5595	1.048	5%	6.2660	0.869	11%

The calculations assume that the superconductor in the wire will have a critical current density $J_c(5T, 4.2K)$ of $2750 A/mm^2$. The quality of the superconductor is degraded when the wires are made in to a cable and put in the magnet. The calculations presented in Table 6.2.7 have been done assuming 5% degradation ($J_c=2612.5$) and 4.35 K bath temperature.

In Table 6.2.7, the field margin (B_{margin}) and the temperature margin (T_{margin}) are listed. The temperature margin is defined as the maximum possible computed rise in the operating temperature (over the design value of normal operation, which is 4.35 K) before

Table 6.2.7: Expected quench performance of the SSC 50 mm dipole with 5% cable degradation ($J_c = 2612.5 A/mm^2$) and at 4.35 K temperature. S_{quench} is the computed current density in the copper at quench and $S_{6.7T}$ at the design field of 6.7 Tesla.

Layer	Cu/Sc	B_{ss}	I_c	B_{margin}	T_{margin}	S_{quench}	$S_{6.7T}$
↓	Ratio	tesla	A	%over 6.7T	kelvin	A/cm^2	A/cm^2
Inner	1.7	7.149	7126	6.7	0.519	736	681
	1.5	7.273	7273	8.6	0.625	788	715
	1.3	7.399	7411	10.4	0.730	853	759
Outer	2.0	7.268	7267	8.7	0.580	919	834
	1.8	7.445	7470	11.1	0.709	980	865

the magnet will quench at the design central field ($B_{design}=6.7$ tesla). The field margin is defined as follows

$$B_{margin} (\%) = \frac{B_{ss} - B_{design}}{B_{design}} \times 100$$

The calculations are done for copper to superconductor ratios, CSR or Cu/Sc, of 2.0 and 1.8 in the outer layer and 1.7, 1.5 and 1.3 in the inner layer. The computed central field (B_{ss}) at the magnet quench point is listed together with the current in the cable at that point (I_c) and the current density (S_{quench}) in the copper available to carry that current after quench. A lower current density in the copper is expected to give better stability. The current density in the copper at 6.7 tesla ($S_{6.7T}$) is also listed. For stability purposes, $S_{6.7T}$ may be a more appropriate parameter to consider than S_{quench} .

The design values selected were a copper to superconductor ratio of 1.8 in the outer layer and of 1.5 in the inner layer. The quench field B_{ss} of 7.273 tesla in the inner layer gives a field margin of 8.6% over the design operating field B_{ss} of 6.7 tesla. The quench field of 7.445 tesla in the outer layer gives a field margin of 11.1%.

6.2.5. Effect of Manufacturing Errors on the Allowed Harmonics

For various reasons, the actual value of a parameter used in designing the coil may turn out to be somewhat different than desired. In particular, deviations in the locations of various turns in the coil are very important. This causes changes in the transfer function and the field harmonics. In this section the effect of these errors in various cases are estimated using a procedure developed by P.A. Thompson [130]. The basic four fold symmetry in the dipole coil geometry is retained in this analysis. Though this is not a realistic assumption, it is useful in estimating the size of some errors. In Table 6.2.8 these effects are listed for a nominal 0.05 mm variation in the given parameter.

First, the change in harmonics due to a change of +0.05 mm in the radius of every turn in each current block, one block at a time, is given. The counting of the blocks in the table starts at the inner layer and at the midplane of each layer. Next the effect of changing the wedge size by +0.05 mm is estimated. Pole angle is held constant in this calculation by reducing the conductor thickness by an appropriate amount. The counting scheme for the wedges is the same as it is for the current blocks. It is possible that during the molding, the thickness of the cable is not reduced uniformly within a layer. To estimate this effect, a linear increase in the cable thickness is assumed going from the midplane towards the pole, followed by a linear decrease, such that the middle turn is displaced azimuthally by 0.05 mm. The pole angle does not change during this perturbation. This effect is given for the inner and outer layers in the next two rows of the table. The effect of increasing the pole angle by 0.05 mm in the inner and in the outer layer is shown in the last two rows. In each group the Root Mean Square (RMS) change of these variations is also given.

Table 6.2.8: The effect of a 0.05 mm increase in the given parameter on the transfer function and the field harmonics.

Parameter changed	TF T/kA	b_2 10^{-4}	b_4 10^{-4}	b_6 10^{-4}
Radius of Block No. 1	0.31	-0.25	-0.10	-0.01
Radius of Block No. 2	-0.32	0.31	0.12	0.01
Radius of Block No. 3	-0.12	0.36	-0.02	-0.01
Radius of Block No. 4	-0.20	0.33	-0.08	0.01
Radius of Block No. 5	-0.11	-0.04	-0.01	0.00
Radius of Block No. 6	-0.78	0.22	0.03	0.00
RMS Blocks	0.38	0.27	0.07	0.01
Thickness of Wedge No. 1	-1.56	-0.48	0.02	0.01
Thickness of Wedge No. 2	0.83	0.59	0.05	-0.01
Thickness of Wedge No. 3	2.32	0.71	-0.04	0.00
Thickness of Wedge No. 4	-0.57	-0.11	0.00	0.00
RMS Wedges	1.48	0.52	0.03	0.01
Cable thickness inner	2.63	1.08	0.05	-0.01
Cable thickness outer	1.99	0.48	0.02	0.00
RMS Cable thickness	2.33	0.83	0.04	0.01
Pole angle inner	-4.01	-0.45	0.06	-0.01
Pole angle outer	-2.26	-0.42	0.00	0.00
RMS Pole angles	3.25	0.43	0.04	0.01

6.2.6. Stored Energy and Inductance Calculations

Stored energy calculations are done with the computer code POISSON [135]. POISSON uses the following formula to compute the stored energy per unit length (E_l) over the cross section area :

$$E_l = \frac{1}{2} \int_a J A_z da,$$

where A_z is the vector potential and J is the current density in the mesh triangle having an area da . The integration needs to be performed only over the regions containing current. At low fields when the field B is proportional to I (i.e. when yoke saturation is not significant), the stored energy is expected to be proportional to B^2 or I^2 .

The stored energy and the inductance are related through the following formula :

$$\text{Stored Energy} = \frac{1}{2} \text{Inductance} \times (\text{Current})^2.$$

The inductance decreases at high field as the iron yoke saturates.

The results of POISSON computations for the SSC 50 mm aperture dipole are given at 6.5 kA in Table 6.2.9 for the stored energy per unit length and the inductance per unit length. The total stored energy and the inductance for a 15 m long dipole are also given.

Table 6.2.9: Stored Energy and Inductance at 6.5 kA as computed with the code POISSON for the SSC 50 mm aperture dipole.

Stored Energy per unit length, kJ/m	105.0
Stored Energy for 15 m long Dipole, kJ	1575.6
Inductance per unit length, mH/m	4.972
Inductance for 15 m long Dipole, mH	74.585

6.2.7. Lorentz Force Calculations

The value of Lorentz force per unit of axial length on each turn is obtained from the components of the magnetic field (B_x, B_y). These components are calculated using program MDP. Since B_x and B_y are not uniform in a turn, an average value of these components is obtained from a grid of 10×2 across the width and thickness of the cable.

The variation in the magnitude of the radial and azimuthal components of the Lorentz forces, namely F_r and F_a (also referred to as F_θ), with turn number is shown in Fig. 6.2.5. The turn numbers are counted from the midplane. The Lorentz force acts on the coil such that the azimuthal component compresses the coil on the midplane and the radial component expands it outward. Though the radial Lorentz force on the turns in the outer layer is very small, the force on the turns in the inner layer must be transmitted through the outer layer to the structure of the magnet.

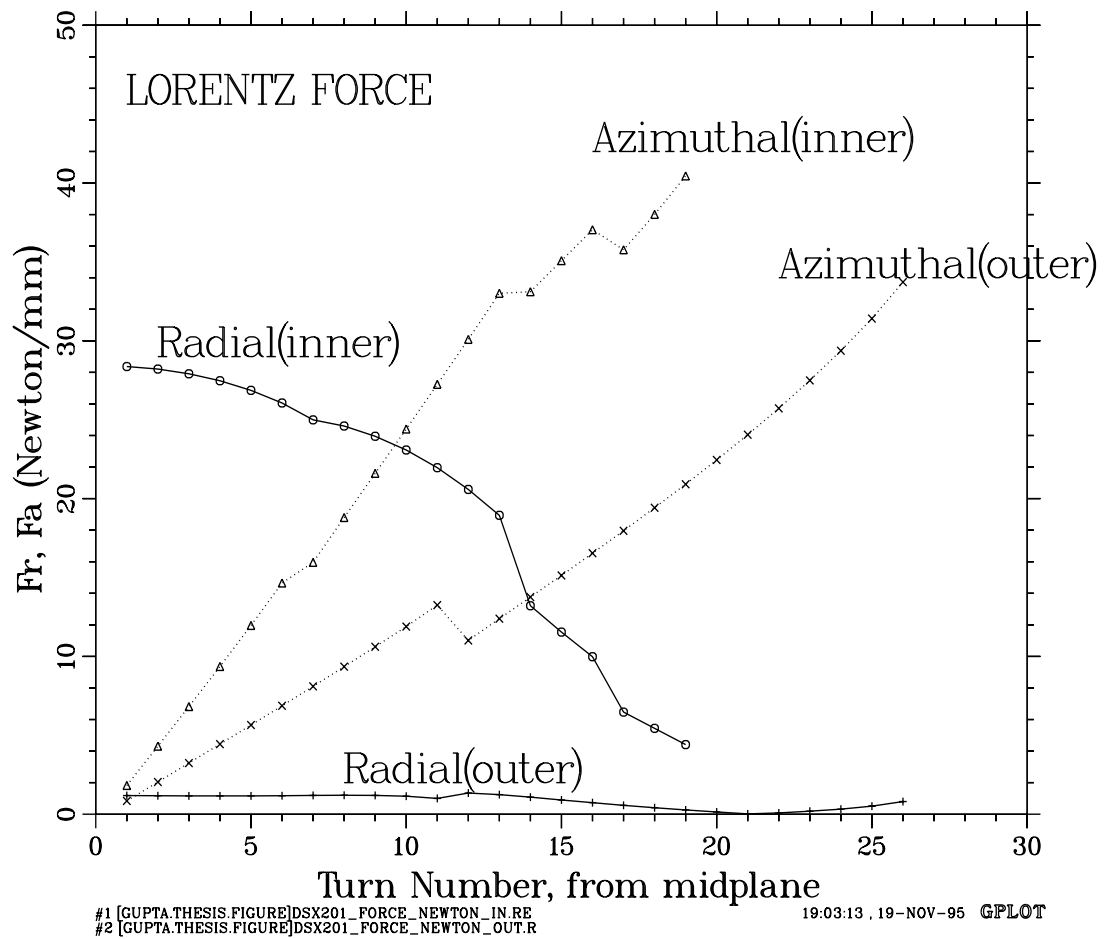


Figure 6.2.5: The magnitude of the components of the Lorentz force on the individual turns in a SSC 50 mm prototype magnet. The radial component of the force (F_r) pushes the coil outward and the azimuthal component (F_a) compresses the coil towards the midplane (horizontal plane). There are 19 turns in the inner layer and 26 turns in the outer layer of each quadrant.

6.2.8. Summary of the Design

A summary of the coil and iron cross-sections are given respectively in Table 6.2.10 and Table 6.2.11. The coil has two layers and the number of turns is the number of turns in the upper or lower half of a layer. The field margin in this cross section is limited by the inner layer. If the cable used in the inner layer had a copper to superconductor ratio of 1.3, the margin would be 10.4% (see Table 6.2.7).

Table 6.2.10: Summary of SSC 50 mm dipole coil cross section.

Layer →	Inner	Outer
No. of Turns	19	26
Strand Diameter, mm	0.808	0.648
Strands per turn	30	36
Coil i.d., mm	49.56	74.91
Coil o.d., mm	75.36	99.42
B_{peak}/B_o	1.048	0.869
Cu/SC	1.5	1.8
Margin over 6.7 T . . .	8.6%	11.1%

Table 6.2.11: Summary of SSC 50 mm dipole iron cross section. $\delta(TF)$ is the change in transfer function, δb_2 in b_2 and δb_4 in b_4 due to saturation.

Inner Diameter, mm	135.6
Outer Diameter, mm	330.2
$\delta(TF)$, at 6.7 T	2.6%
δb_2 , prime unit	0.3
δb_4 , prime unit	0.03

6.3. RHIC 130 mm Aperture Interaction Region Quadrupole Cross-section

A total of seventy two, 130 mm aperture quadrupoles are required in six interaction regions of RHIC. Each interaction region includes 4 sets of quadrupole triplets (see Fig. 5.2.11 which shows one of two beam lines at an intersection). The Q1, Q2 and Q3 quadrupoles in each triplet have the same cross section, and magnetic lengths, respectively, of 1.44 m, 3.4 m and 2.1 m. The major parameters of these quadrupoles are shown in Table 6.3.1.

The particle beam is focussed to a small size at the crossing point in the two low-beta ($\beta^*=1$) interaction regions to obtain a high luminosity. An unavoidable consequence of this squeeze is the increase in the beam size in these quadrupoles. Moreover, the rapid variation in beam size within the focusing triplet limits the effectiveness of the local and lumped global corrector system [171]. Therefore, good field quality in these quadrupoles is crucial to the high luminosity operation of RHIC. Since the maximum luminosity is desired at the top energy, the field errors are designed to be minimized at the maximum operating gradient.

6.3.1. Basic Construction

The cross section of the cold mass is shown in Fig. 6.3.1. Following the design philosophy used in most other RHIC magnets, the yoke is used here as a collar to compress the coils. The yoke aperture consists of concentric circular arcs with two radii instead of the usual circular aperture. As explained in chapter 2, this reduces the b_5 saturation by over an order of magnitude. The space between the coil and the yoke is filled with a thin, glass-filled phenolic spacer. The spacer has two radii for the outer surface which closely follows the geometry of the yoke inner surface. However, at eight places a gap is left between the yoke and spacer where partially magnetic tuning shims are placed to correct the measured field harmonics after the coils are assembled in the yoke. The tuning shims are discussed in more detail in a previous chapter. A 6.35 mm thick stainless steel shell enclosing the yoke is welded together after the collaring keys are inserted in the compressed yoke. The quadrupoles of the inner and outer rings share a common cryostat. The minimum center-to-center distance between adjacent Q1 quadrupoles is 424 mm.

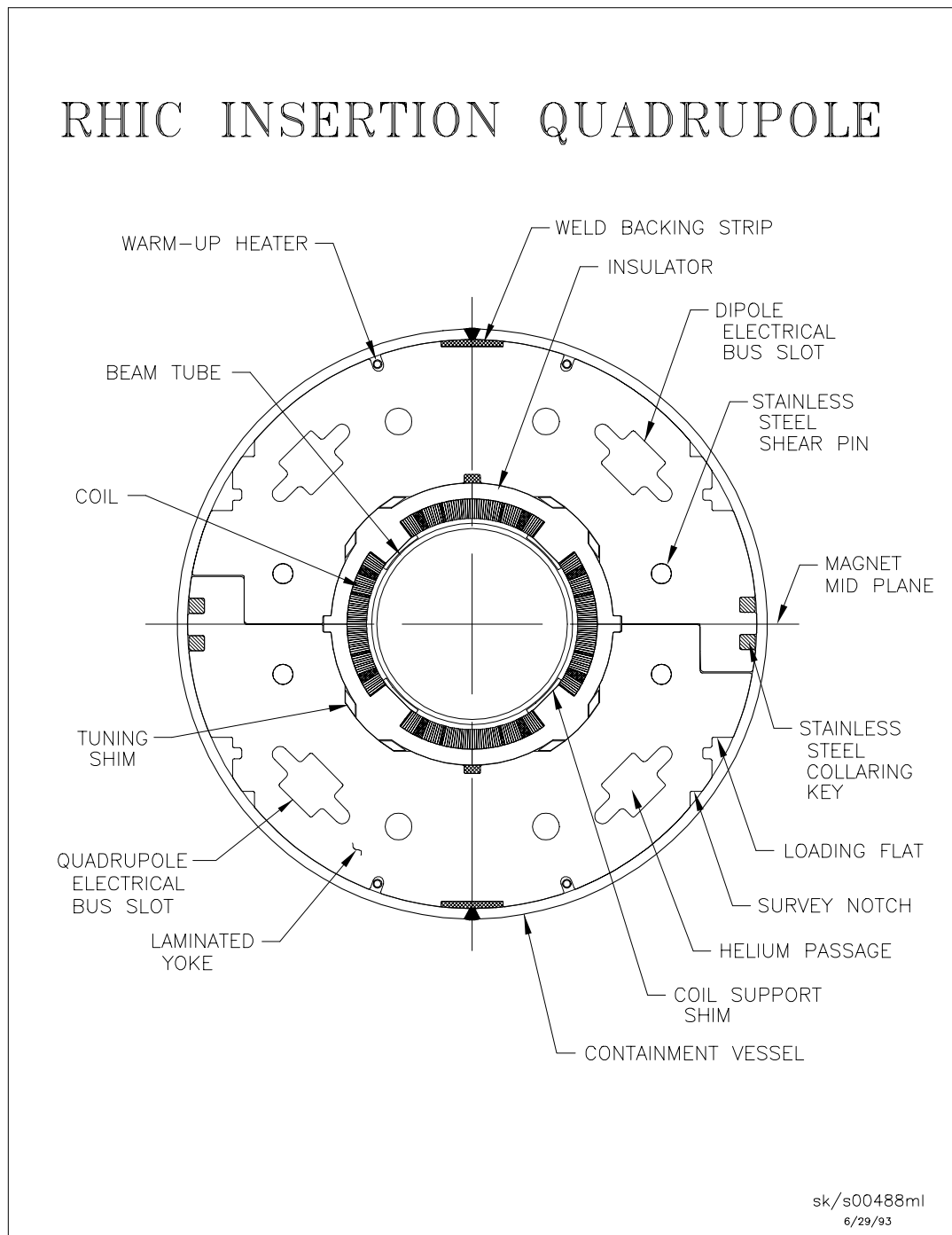


Figure 6.3.1: Cross section of the 130 mm aperture quadrupoles for a RHIC interaction region.

Table 6.3.1: The basic design parameters of the 130 mm aperture quadrupoles for the RHIC interaction regions.

Parameter	Value
Superconducting wire diameter	0.65 mm
Number of wires per cable	36
Copper to superconductor ratio	1.8
Cable mid-thickness	1.16 mm
Cable width	11.7 mm
Cable insulation	Kapton CI
Critical current at 5.6T, 4.2 K	≥ 10100 A
Number of turns per pole	27
Coil inner radius	65 mm
Coil outer radius	77 mm
Yoke lamination thickness	6.35 mm
Yoke inner radius at midplane	87 mm
Yoke inner radius at pole	92 mm
Yoke outer radius	175.26 mm
Magnetic length, Q1, Q2, Q3	1.44, 3.4, 2.1 m
Stored energy in Q2 magnet	165 kJ
Minimum beam spacing in triplet ..	424 mm
Maximum design current	5.05 kA
Maximum design gradient	48.1 T/m
Operating temperature	4.6 K
Computed quench current at 4.6 K	8.26 kA
Computed quench gradient at 4.6 K	75.3 T/m
Gradient margin	57%

Table 6.3.2: The basic coil design parameters of the 130 mm aperture quadrupoles for the RHIC intersection regions. The harmonics b_n for the final cross section are given at 40 mm reference radius. “Circular iron aperture” rows show the expected harmonics for a circular iron aperture with a yoke inner radius of 87 mm. “Actual iron aperture” rows show the expected harmonics for the two radii (87 mm and 92 mm) design. The table also includes the harmonics due to nominal tuning shims and the effect of the asymmetric deformation in the yoke aperture during collaring.

Parameter	Value
Number of layer(s)	1
Number of wedges	2
Turn configuration (from midplane) .	13, 8, 6
Wedge 1, Min./Max. thickness, mm .	1.143/1.143
Wedge 2, Min./Max. thickness, mm .	4.227/6.35
Coil-to-midplane gap (0°, 180°), mm .	0.356 mm
Coil-to-midplane gap (90°, 270°), mm	0.279 mm
Coil inner radius	65 mm
Coil outer radius	77 mm
b_3 for circular iron aperture	3.0
b_3 for actual iron aperture	0.0
b_5 for circular iron aperture	-29.6
b_5 for actual iron aperture	-1.2
b_7 for circular iron aperture	-0.22
b_7 for actual iron aperture	-0.1
b_9 for circular iron aperture	1.1
b_9 for actual iron aperture	0.0

6.3.2. Coil Cross Section

One octant of the coil cross section is shown in Fig. 6.3.2. The coil has a total of 27 cables per octant in three blocks. The coil is designed using a superconducting cable which is used in the outer layer of the SSC 50 mm dipole magnet (see Table 6.2.1). This cable is

$\sim 20\%$ wider than the one which is used in the RHIC arc dipole and quadrupole magnets. The additional superconductor in this wider cable gave a sufficient margin over the original design gradient of 59 T/m in a single layer coil. As shown, in Table 6.3.1, the design gradient in the present RHIC lattice has been reduced to 48.1 T/m. The specifications for the critical current I_c at 4.2 K and at 5.6 T in wire and in cable are respectively 286 A and 10100 A. The cable is almost fully keystoneed for the 130 mm coil aperture.

The coil is optimized using the computer program PAR2DOPT [130]. This is an analytic program which computes and optimizes field harmonics for a coil in a circular iron aperture. As mentioned earlier, the iron aperture is not circular in this design. This means that a coil optimized for zero harmonics in a circular aperture would have non-zero harmonics here. Therefore, the coil is designed with non-zero harmonics in a circular aperture to cancel the harmonics generated by this non-circular iron aperture. These required non-zero values (also referred to as offsets) are computed using the code POISSON.

The optimized coil cross section is shown in Fig. 6.3.2. The coil has 27 turns in the three blocks (two wedges) of each octant with the distribution of the number of turns in the three blocks being 13, 8 and 6. The two wedges are mechanically symmetric. In addition, the smaller wedge (the one which is closer to the midplane) is rectangular. The various mechanical and magnetic parameters of this cross section are shown in Table 6.3.2. The presence of b_3 and b_7 , which are normally non-allowed harmonics in quadrupoles, is discussed later. In addition to low harmonic content and a lower value of maximum field on the conductor, this particular cross section was chosen for its good flexibility (tunability) in accommodating changes in field harmonics and mechanical parameters such as the thickness of the cable.

The good tunability of coil cross section and the one rectangular wedge turned out to be very useful in obtaining a good field quality in pre-production model magnets when a decision to change the cable insulation was made. The new Kapton-CI insulation increased the thickness of the insulated cable by 0.023 mm compared to the original design. This would have resulted in an 0.635 mm increase in coil size since there are 27 turns in the cross section. This is about an order of magnitude more than the tolerance required to maintain the desired pre-compression on the coils. However, since the shape of one of the wedges was rectangular, it could be easily rolled to a 0.635 mm smaller size. This reduction in wedge size compensated for the thicker insulation, and the original coil size and coil pole angle in the magnet could be maintained. This avoided an adjustment in the number of

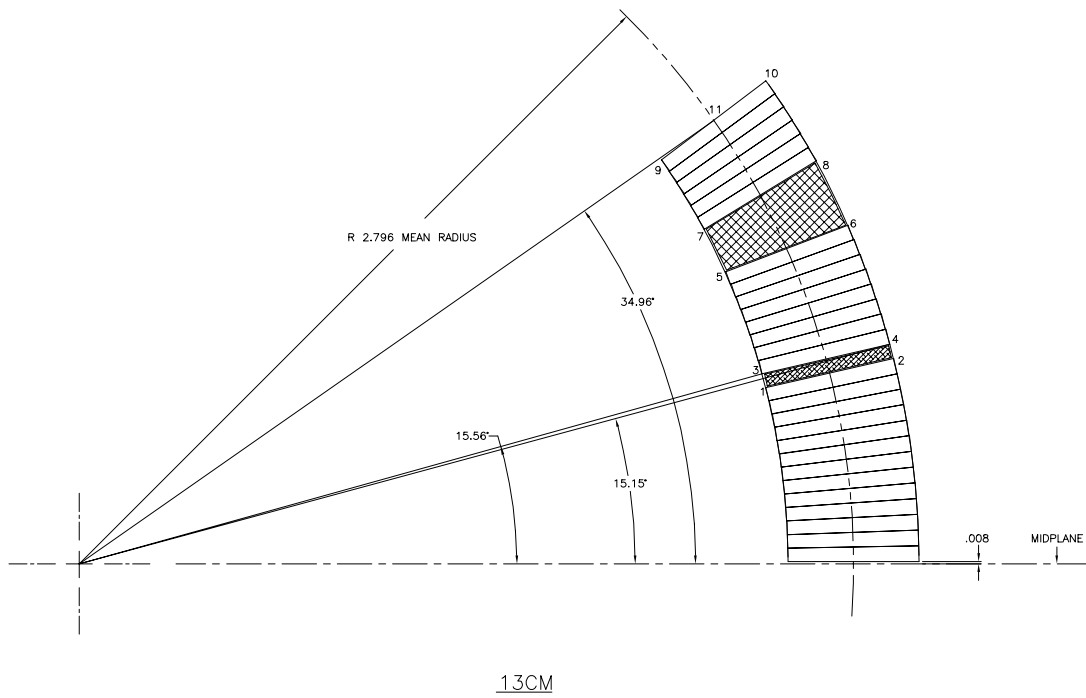


Figure 6.3.2: Optimized coil cross section for the RHIC 130 mm aperture insertion quadrupole.

parts in the body and the end section of the magnet. In this selected cross section, the above change did not produce a significant change in b_5 , the first allowed harmonic with quadrupole symmetry. This straightforward accommodation of a large mechanical change without a corresponding deterioration in the field quality was possible only because the cross section was optimised and chosen to permit such tunability. The value of the next allowed harmonic b_9 , created by the large change, is about 1 unit. This was removed in the next iteration.

In an attempt to maximize the use of existing tooling, these quadrupoles are collared like dipoles. However, during the collaring an elliptical deformation is created in the iron and also in the coil since the yoke inner surface defines the coil outer surface. The turns on the horizontal axis are displaced inward and an overall ovality is created as the vertical axis tends to elongate. This deformation breaks an ideal quadrupole symmetry and creates the non-allowed harmonics b_3 , b_7 , etc. A large value (~ 6 unit) of b_3 harmonic was observed in the pre-production quadrupoles due to this yoke deformation (asymmetry). A method was developed to remove the harmonics created by this asymmetry. A deliberate difference between the horizontal and vertical midplane gap (see Table 6.3.2) in the coil cross section was introduced. This difference in midplane gap breaks the horizontal/vertical symmetry in the coil cross section and generates the harmonics b_3 , b_7 , etc. The amount of this second asymmetry (coil asymmetry) can be adjusted to properly compensate for the first asymmetry (yoke asymmetry) created in the collaring press. The calculations and measurements showed that if the half-gap on the horizontal midplane is made about 0.1 mm larger than the half-gap on the vertical midplane, then the b_3 due to yoke asymmetry can be compensated. This was incorporated in eight quadrupoles. However, the asymmetry in coil assembly also produces a small (-0.35 unit) but significant b_7 . Therefore, in later magnets, only part of the correction is applied using this method. The rest is obtained using magnetic tuning shims. The sign of b_3 and b_7 in the two methods is opposite. Therefore, in principle when an asymmetric midplane shim is used in conjunction with the magnetic tuning shims, both b_3 and b_7 could be made zero. However, that would take away a significant part of the tuning shim capacity which could be used to compensate other harmonics. In the final design the target b_3 is zero and b_7 is about -0.1 unit.

6.3.3. Yoke Cross Section

In cosine θ magnets, the iron aperture is circular. However, in order to reduce the b_5 due to saturation the conventional circular shape has been modified in this design. The yoke aperture is defined by arcs of two concentric circles having radii of 87 mm at the midplane and 92 mm at the pole. This method has been very effective in reducing the b_5 due to saturation from 15 to 1 unit. The basic principle behind it is that it forces an early saturation at the yoke midplane (unless the yoke outer diameter is too large) and delays/reduces the saturation at the pole. Saturation control holes which were found very effective in dipoles are not so effective in the quadrupoles. The nominal transition from 87 to 92 mm occurs at about 30 degrees in the first octant (the angle in the other octants is defined by quadrupole symmetry). At $\theta = 30$ degree (and similarly in other octants) there is a straight face perpendicular to the midplane, extending from the smaller yoke radius of 87 mm to the larger iron radius of 92 mm. The position angle and the difference between these two radii are used as parameters in the optimization process to reduce the b_5 saturation. The size of the locating notch, shown in Fig. 6.3.1, at the midplane of the yoke aperture is 5 mm deep and 10 mm wide. Four slots – two for helium bypass and two for bus work – are located symmetrically at 45° , 135° , 225° and 315° as shown in the figure. The size, shape and location of these slots are determined by the magnetic, mechanical and cooling requirements. Other structures in the yoke are also shown in the figure. Though several of these structures break a strict 8-fold quadrupole symmetry, their location is such that their influence on the iron saturation is minimal. These structures include the holes in the yoke for the stainless steel (non-magnetic) pins and and cutouts for the stainless steel keys. The results of computer calculations show that these holes and cutouts in the yoke generate symmetry breaking harmonics of less than 0.1 unit in the design range of operation. The presence of another quadrupole in the other ring may influence the field at the center of the magnet at high currents. This would be a maximum when the separation between the two magnets is a minimum. Moreover, it is maximum when both of these magnets run at the same high gradient. Computer calculations show that these cross talk induced harmonics are less than 0.1 unit.

The calculations have been performed using the computer codes POISSON, PE2D and MDP. Good agreement has been found between the results obtained by these three codes; this is important because the yoke saturation has been significantly altered in this design by the 2-radius aperture. A computer model of one quadrant of the magnet for the code

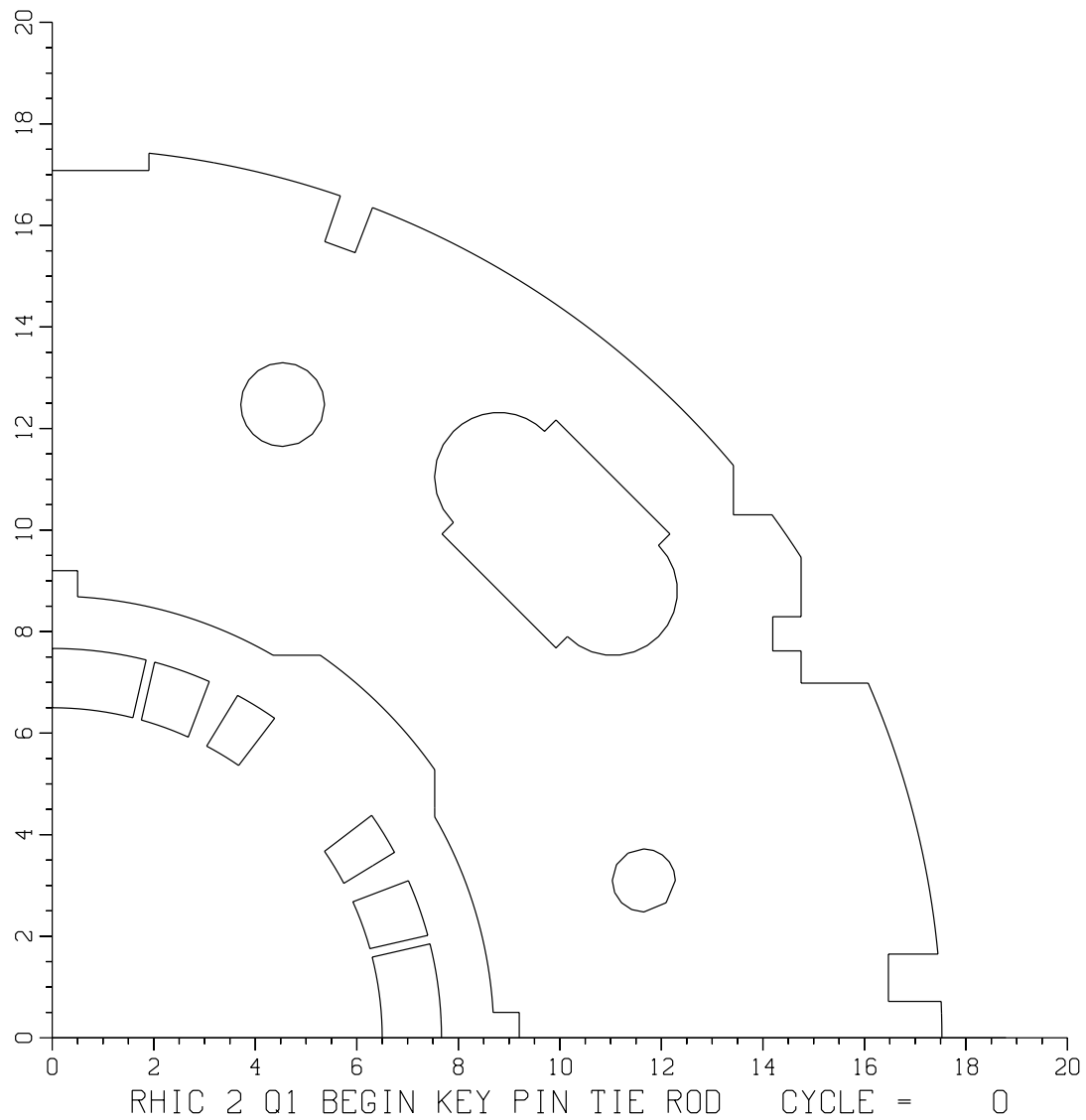


Figure 6.3.3: POISSON model for 1/4 of the cold mass cross section of the RHIC 130 mm aperture insertion quadrupole. The rest of the cold mass is described by the symmetry. A perfect quadrupole has an eight fold symmetry; this is partly broken here by the yoke split on the horizontal midplane.

Table 6.3.3: Harmonics in the straight section of the RHIC 130 mm aperture insertion quadrupoles as computed for a POISSON model of a quadrant of the magnet. The harmonics are given at 40 mm radius. $\infty\mu$ represents the calculations when the permeability in the iron is assumed to be ∞ . *Grad* denotes the field gradient. A dependence of the harmonics b_3 and b_7 on the current reflects the absence of an ideal 8-fold quadrupole symmetry.

I	<i>Grad</i>	T.F.	b_3	b_5	b_7	b_9	b_{11}	b_{13}
kA	T/m	T/m/kA	10^{-4}	10^{-4}	10^{-4}	10^{-4}	10^{-4}	10^{-4}
$\infty\mu$	$\infty\mu$	9.574	0.00	-1.20	0.00	-0.10	0.00	0.0
1.0	9.5730	9.573	0.00	-1.22	0.00	-0.10	0.00	0.00
3.0	28.7165	9.5722	0.00	-1.23	0.00	-0.10	0.00	0.00
4.0	38.2583	9.5646	0.03	-1.16	-0.01	-0.05	-0.01	0.00
5.0	47.6639	9.5328	0.10	-1.11	0.00	0.13	-0.01	-0.01
5.5	52.2567	9.5012	0.15	-1.28	-0.01	0.26	0.00	-0.01
6.0	56.7096	9.4516	0.10	-1.36	-0.02	0.39	0.00	-0.01
6.5	60.9980	9.3843	0.08	-1.32	-0.03	0.52	0.00	-0.01
7.0	65.1189	9.3027	0.04	-1.58	-0.04	0.63	-0.01	-0.01
7.5	69.0485	9.2065	0.02	-2.40	-0.05	0.72	-0.01	0.00
8.0	72.8282	9.1035	-0.11	-3.70	-0.07	0.78	-0.01	0.00
8.5	76.5207	9.0024	-0.40	-5.21	-0.09	0.83	-0.01	0.01
9.0	80.1618	8.9069	-0.65	-6.76	-0.10	0.86	-0.01	0.01
9.5	83.7541	8.8162	-0.76	-8.30	-0.11	0.88	-0.01	0.02

POISSON is shown in Fig. 6.3.3. The results of calculations showing the current dependence of the harmonics allowed by the actual geometry are given in Table 6.3.3. The harmonics b_3 , b_7 and b_{11} are not allowed in a strictly 8-fold quadrupole symmetry. The dependence of them on current reflects the absence of the ideal 8-fold symmetry. The yoke is designed such that the magnitude of these harmonics is small even at high currents. The computed dependence of the harmonics b_3 , b_5 and b_9 on current is plotted in Fig. 6.3.4.

The calculations described above are for one magnet by itself, i.e. no other magnet is present in the vicinity. However, in the layout of the RHIC lattice, there is always another 130 mm aperture quadrupole located nearby. The minimum separation between the outer yoke diameter of the two is ~ 73.5 mm. The thickness of the iron yoke in these quadrupoles, though sufficient to contain the field lines at the design current, is not sufficient to contain them at the quench current of 8.26 kA. In this situation, the non-allowed harmonics show a dependence on current at high field. This is commonly referred to as cross talk and it implies that the field of one magnet is influencing the field in the aperture of the other magnet.

In RHIC, the ratio of rigidities of the two counter rotating beams varies in the range of 1:1 to 1:0.4. That means that the excitation of two side-by-side quadrupoles can, in general, be different. The direction of the field in the two is the same. In this case, the amount of cross talk between the two quadrupoles is a maximum when both are excited at the same high current (1:1 case). Therefore, in the calculations presented here for the non-allowed field harmonics, only the 1:1 case is considered. The cross talk is a maximum at the Q1 location where the two quadrupoles are at their minimum separation, with a center-to-center distance being 424 mm. Moreover, since the two quadrupoles at the Q1 location are not parallel to each other, the separation (and hence the amount of cross talk) between them is different at the two ends of these magnets. The non-allowed harmonics (in particular b_o , which is affected the most) are a maximum when the separation between the two quadrupoles is a minimum. The results of calculations for this case using the code POISSON are given in Table 6.3.4. The maximum operating current in the present design is about 5.05 kAmp. The amount of cross talk is negligible in the design range of operation and is very small up to the expected quench current (8.26 kA). The field lines at quench in one of two side-by-side quadrupoles are shown in Fig. 6.3.5 (the other quadrupole, not shown, is on the left side of the one shown).

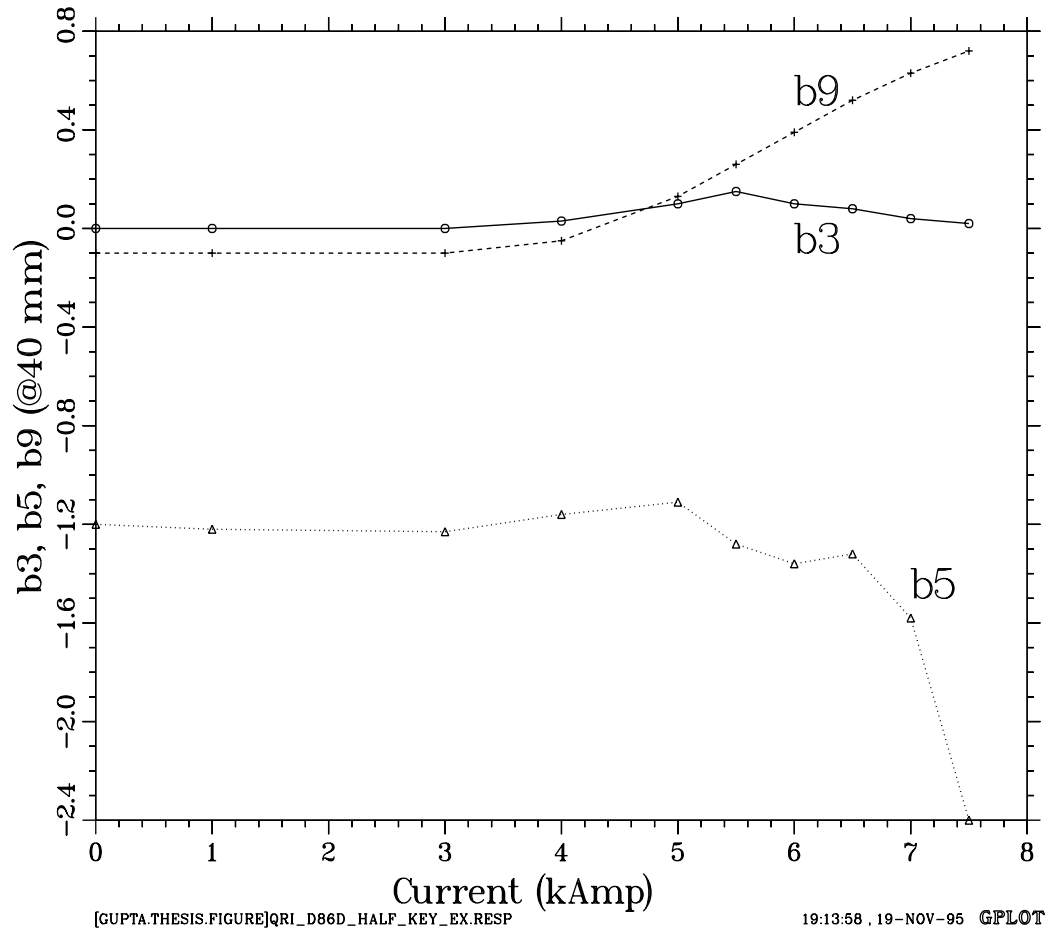


Figure 6.3.4: Variation in the b_3 , b_5 and b_9 harmonics as a function of current in 130 mm aperture RHIC insertion quadrupole as computed with the code POISSON. The computer model is shown in Fig. 6.3.3.

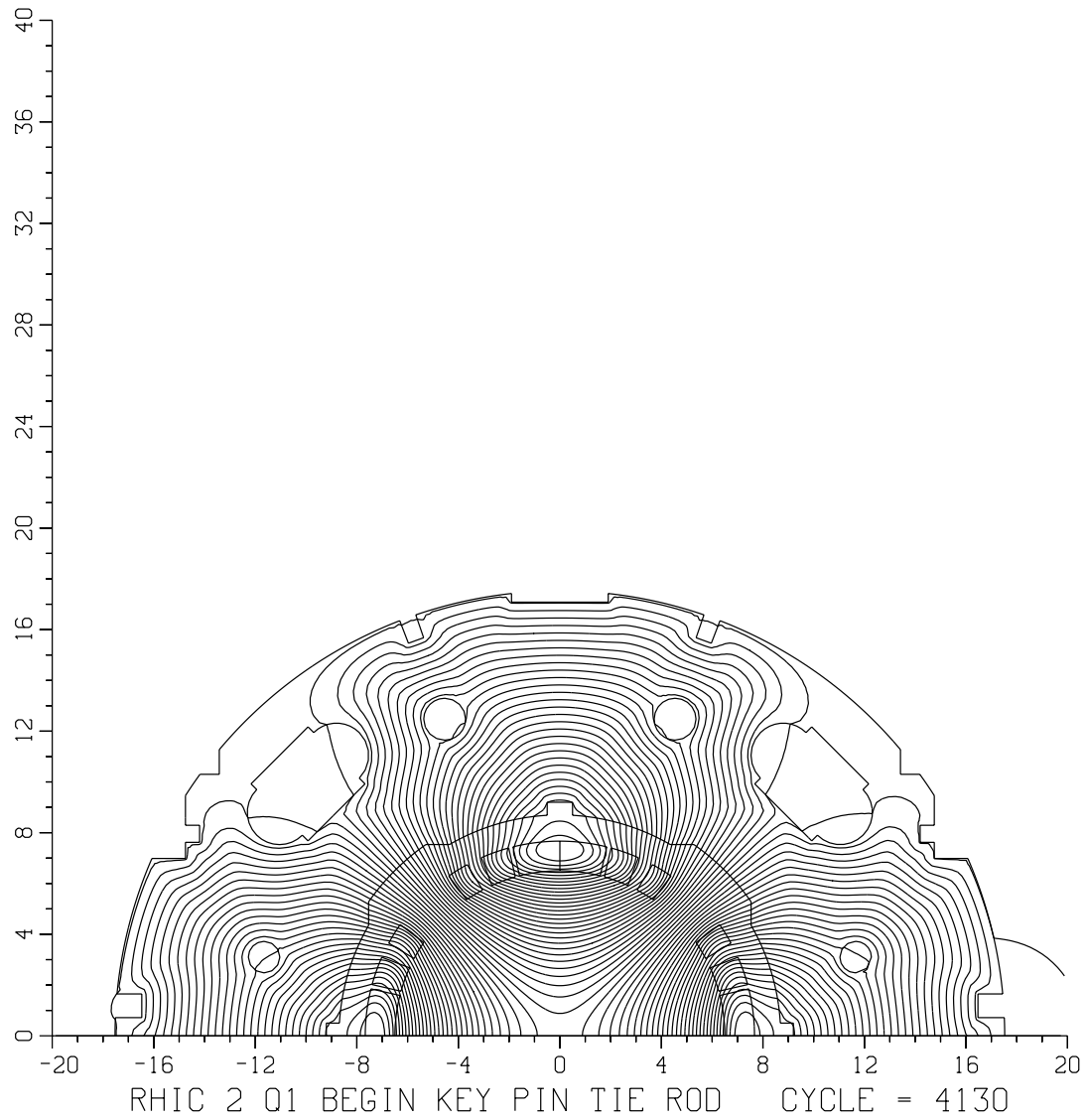


Figure 6.3.5: The field lines at quench in one of two side-by-side quadrupoles. The other quadrupole, not shown, is on the left side of the one shown. The minimum center to center distance between the two quadrupoles is 42.4 cm.

Table 6.3.4: Harmonics in the straight section of the RHIC 130 mm aperture quadrupoles at the Q1 location where the separation between the two side-by-side quadrupoles is a minimum (424 mm). The harmonics are given at 40 mm radius. $\infty\mu$ represents the calculations when the permeability in the iron is assumed to be ∞ . *Grad* denotes the field gradient. These computations are made using the code POISSON.

I	<i>Grad</i>	T.F.	b_0	b_2	b_3	b_4	b_5	b_6	b_7	b_8	b_9
kAmp	T/M	T/M/kA	10^{-4}	10^{-4}	10^{-4}	10^{-4}	10^{-4}	10^{-4}	10^{-4}	10^{-4}	10^{-4}
$\infty\mu$	$\infty\mu$	9.5742	0.00	0.00	0.00	0.00	-1.20	0.00	-0.10	0.00	0.00
1.0	9.5735	9.5735	-0.03	0.01	0.01	0.01	-1.22	0.01	-0.10	0.00	0.00
3.0	28.7171	9.5724	-0.03	0.02	0.00	0.01	-1.23	0.01	-0.10	0.00	0.00
4.0	38.2591	9.5648	0.14	0.02	0.07	-0.02	-1.16	0.01	-0.11	0.01	0.05
5.0	47.6671	9.5334	0.14	0.01	0.05	-0.02	-1.09	0.01	-0.11	0.01	0.24
5.5	52.2588	9.5016	0.14	0.07	0.05	-0.02	-1.25	0.01	-0.12	0.00	0.37
6.0	56.7113	9.4519	0.25	0.08	0.03	-0.01	-1.33	0.01	-0.13	0.01	0.50
6.5	61.0000	9.3846	0.13	0.03	0.01	0.01	-1.31	0.01	-0.14	0.01	0.63
7.0	65.1185	9.3026	0.42	0.05	-0.02	0.02	-1.60	0.01	-0.15	0.01	0.74
7.5	69.0458	9.2061	0.82	0.09	-0.01	0.04	-2.44	0.01	-0.15	0.01	0.83
8.0	72.8246	9.1031	1.61	0.19	-0.16	0.07	-3.74	0.02	-0.17	0.01	0.89
8.5	76.5132	9.0016	2.78	0.32	-0.47	0.12	-5.27	0.03	-0.19	0.01	0.93
9.0	80.1467	8.9052	4.06	0.46	-0.73	0.17	-6.84	0.03	-0.21	0.01	0.97
9.5	83.7381	8.8145	5.53	0.59	-0.87	0.22	-8.40	0.04	-0.21	0.01	0.990

6.3.4. Expected Quench Performance

To compute the gradient at quench, the maximum field on the conductor (the peak field) is first calculated. The location of the peak field is on the pole-most surface of the pole turn. It is 16% radially outward from the coil inner radius. The value of this field together with the gradient at 7000 A and 8000 A is given in Table 6.3.5.

Table 6.3.5: Peak field on the cable in the 130 mm aperture quadrupole. The peak field in the coil is on the pole turn.

Current	Gradient	Field
7000 A	65.07 T/m	4.991 T
8000 A	73.16 T/m	5.626 T

The specification for the critical current in the wire is ≥ 286 amperes at 4.2 K temperature and 5 Tesla field. In this 36 strand cable, after a 2% degradation, the minimum critical current in the cable is specified to be 10,100 amperes. This gives a computed quench gradient of 75.3 T/m at 4.6 K, which is 57% over the design value of 48.1 T/m. The computed quench current is 8260 amperes which is ~ 64 % above the design value of 5050 amperes. The current density in the copper at quench is 1133 A/mm² and at design field is about 670 A/mm². The critical current in the cable actually used in manufacturing the magnets is about 12,000 ampere, which is much better than the minimum specified value. This would give a quench gradient of 80.1 T/m and quench current of 8860 ampere.

6.4. Conclusions on the Optimized Cross Section Designs

It is shown in this chapter that the methods described in the previous four chapters can be implemented to design and construct high field quality magnets. These methods have been used in the magnetic design of the cross section for the prototype of the SSC 50 mm aperture collider dipole magnets built at BNL and Fermilab. These methods are also used in the design of a number of magnets for RHIC but only the design of the 130 mm aperture quadrupole magnets has been included here to describe the procedure in fair detail.

A good design would require that besides being optimized for field quality, the cross section is also optimized to give a high quench field, to incorporate the required cooling and mechanical considerations and to simplify the manufacturing to make it as error free as possible. For example, the copper wedges are made completely symmetric in the inner layer of the SSC 50 mm aperture design (and in both layers in the Fermilab design) and the two nearly equal size wedges are made exactly equal. In the RHIC 130 mm aperture quadrupole design, not only are the wedges symmetric but the smaller of the two wedges is rectangular. None of these mechanical manufacturing considerations resulted in a degradation in field quality; it merely required optimizing the cross section design with certain guidelines.

In the SSC 50 mm dipole magnet design, the iron saturation is controlled by choosing the size, location and material of the yoke-yoke alignment key at the midplane for the BNL-built, horizontally split yoke design. In the Fermilab-built, vertically split design a cutout is introduced at the midplane to obtain similar performance. The iron saturation in the RHIC insertion quadrupoles is controlled by the 2-radius method.

The RHIC 130 mm aperture quadrupoles are collared with a 2-fold symmetry. The collaring process creates an elliptical-type deformation which creates a large b_3 harmonic. This can be removed by making the coil midplane gap larger at the horizontal plane than at the vertical plane. This, however, creates a b_7 harmonic. It is shown that a proper combination of an asymmetric midplane gap and an asymmetric tuning shim (which also creates a b_7 but with opposite sign) makes both b_3 and b_7 small.